Mussel-Inspired Multifunctional Hydrogel Coating for Prevention of Infections and Enhanced Osteogenesis

Hao Cheng,[†,‡,§] Kan Yue,[†,‡] Mehdi Kazemzadeh-Narbat,[†,‡] Yanhui Liu,[†,‡,∥] Akbar Khalilpour,[†,‡] Bingyun Li,[⊥] Yu Shrike Zhang,[†,‡] Nasim Annabi,*[,†,‡,#] and Ali Khademhosseini*[,†,‡,∇,○]

[†]Biomaterials Innovation Research Center, Division of Biomedical Engineering, Department of Medicine, Brigham and Women's Hospital, Harvard Medical School, Cambridge, Massachusetts 02139, United States

[‡]Harvard−MIT Division of Health Sciences and Technology, Massachusetts Institute of Technology, Cambridge, Massachusetts 02139, United States

[§]Othopeadic Department, Tongji Hospital, Tongji Medical College, Huazhong University of Science and Technology, Wuhan 430030, China

[∥]College of Textiles, Donghua University, Shanghai, 201620, China

[⊥] Department of Orthopaedics, School of Medicine, West Virginia University, Morgantown, West Virginia 26506, United States

[#]Department of Chemical Engineering, Northeastern University, Boston, Massachusetts 02115-5000, United States

[∇]Department of Bioindustrial Technologies, College of Animal Bioscience and Technology, Konkuk University, Seoul, 143-701, the Republic of Korea

[○]Department of Physics, King Abdulaziz University, Jeddah 21569, Saudi Arabia

S *Supporting Information*

ABSTRACT: Prevention of postsurgery infection and promotion of biointegration are the key factors to achieve long-term success in orthopedic implants. Localized delivery of antibiotics and bioactive molecules by the implant surface serves as a promising approach toward these goals. However, previously reported methods for surface functionalization of the titanium alloy implants to load bioactive ingredients suffer from time-consuming complex processes and lack of long-term stability. Here, we present the design and characterization of an adhesive, osteoconductive, and antimicrobial hydrogel coating for Ti implants. To form this multifunctional hydrogel, a photo-cross-linkable gelatin-based hydrogel was modified with catechol motifs to enhance adhesion to Ti surfaces and thus promote coating stability. To induce antimicrobial and osteoconductive properties, a short cationic antimicrobial peptide (AMP) and synthetic silicate nanoparticles (SNs) were introduced into the hydrogel formulation. The controlled release of AMP loaded in the hydrogel demonstrated excellent antimicrobial activity to prevent biofilm formation. Moreover, the addition of SNs to the hydrogel formulation enhanced osteogenesis when cultured with human mesenchymal stem cells, suggesting the potential to promote new bone formation in the surrounding tissues. Considering the unique features of our implant hydrogel coating, including high adhesion, antimicrobial capability, and the ability to induce osteogenesis, it is believed that our design provides a useful alternative method for bone implant surface modification and functionalization.

KEYWORDS: adhesive hydrogels, titanium implant, antimicrobial, osteogenesis, silicate nanoparticles
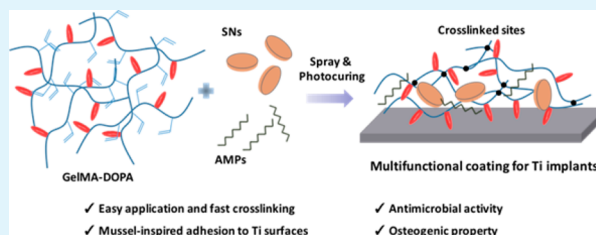
1. INTRODUCTION

Orthopedic implants based on Ti or Ti alloys have been extensively used in clinics due to their superior mechanical characteristics and biocompatibility.[1−3] However, the long-term usage of implants is often compromised due to persistent postsurgical infections, which are challenging to treat and could eventually lead to replacement of the prostheses.[4,5] Controlled localized delivery of certain antibiotics loaded in the coating layer of the implants has been proposed as a promising strategy to prevent implant-associated infections and failure. Several different methods have been reported to introduce antibiotics on the surface of the implants. For example, silver nanoparticles have been loaded on implant surfaces to provide antimicrobial activities.[6,7] Moreover, a short cationic antimicrobial peptide (AMP) known as HHC-36 has also been investigated as an antimicrobial component for Ti implant surface modification, due to its wide-spectrum antimicrobial activity against common Gram-positive and Gram-negative bacteria with enhanced efficacy compared to traditional antibiotics.[8−11] However, these reported methods are generally time-consuming and

require complex multistep procedures to achieve surface modification and drug loading.[6,9,10,12,13]

Another important requirement for successful long-term bone implant is the proper osteointegration between the implant and the surrounding tissues.[14] Although it has been demonstrated that cells can adhere and spread on Ti substrates with a TiO$_2$ layer, Ti metals are generally considered bioinert. As a result, introduction of bioactive molecules on Ti surfaces has been explored to enhance cell functions, to direct new tissue formation, and to promote biointegration.[15,16] Previously, many different bioactive ingredients have been used for the surface modification of Ti implants to promote tissue integration and healing. For example, the introduction of Arg-Gly-Asp (RGD) short peptide could enhance adhesion and function of osteoblasts.[17] Besides, the immobilization of inorganic nanoparticles,[15] growth factors,[15,18] and microRNA-loaded nanocapsules[19] has been shown to enhance bone regeneration.

For clinical applications, it would be ideal to achieve the surface modification of Ti implants by simple procedures, for example, spraying a drug-loaded solution onto the implant immediately before the surgery, which can form a coating layer strongly binding to the implant in situ with enhanced coating stability. It is also preferred to be able to simultaneously load multiple bioactive components with different physical characteristics (such as peptides and inorganic nanoparticles) on Ti surfaces within a single modification step. This will allow feasible introduction of different functions (e.g., antimicrobial activities, motifs for cell adhesion, growth factors to direct cell differentiation) and subsequent optimization of potential synergetic positive effects from each component. Up to now, it is still quite challenging to achieve these goals.

Chemically cross-linked hydrogels could serve as the matrix for the surface modification, given their insolubility to resist washing away by body fluids. In particular, photo-cross-linkable hydrogels provide the option to first spray the prepolymer solution onto the implants, followed by in situ photo-cross-linking to cure the coating layer.[12,20,21] However, to achieve long-term stability, hydrogels should possess strong adhesion to Ti surfaces, especially under wet environments. Inspired by the unusual ability of mussels to adhere to essentially any surfaces under water, extensive studies in the past few decades suggest that the presence of catechol motifs contributes to improved adhesion.[22,23] Since then, mussel-inspired biomaterials have been extensively studied for various applications, including developing a general coating strategy,[24] designing strong adhesives under wet conditions,[25,26] and fabricating hybrid composite nanoparticles,[27] among many others.[28−30] In particular, mussel-inspired hydrogels have been demonstrated to possess unique properties, such as being highly adhesive, self-healing, pollutant absorbing, and antifouling.[30] Especially, in the case of surface modification of inorganic Ti implants, the unique strong and reversible coordination bonds between Ti atoms and the catechol motifs could further enhance the binding strength.[23] Recently, catechol-containing synthetic polymers have been demonstrated to form adhesive coating layers on metal substrates following simple spin-coating techniques,[31] which can be used as load-bearing glues at the metal−plastic interfaces.

To combine the desirable features, such as easy application, antimicrobial activity, and regenerative capability, we propose to develop a mussel-inspired, adhesive, and biocompatible hydrogel coating that can be cross-linked in situ after spraying onto the implant surfaces.[30] Antimicrobial drugs and other bioactive ingredients can be physically loaded into this hydrogel to achieve controlled delivery after surgery. We proposed to use gelatin methacryloyl (GelMA), which has been popularized in the field of tissue engineering and regenerative medicine,[16,32−34] as a regenerative hydrogel material. Further functionalization of GelMA hydrogels with catechol motifs can enhance the binding affinity with Ti surfaces. To introduce antimicrobial activity, we selected the AMP to be loaded into the hydrogel with controlled release capability.[8−11] Moreover, we added osteoconductive silicate nanoparticles (SNs), commercially available as Laponite nanosilicates, into the hydrogel formulation to promote bone healing. These synthetic Laponite SNs are anionic nanoplates with a diameter around 30 nm and a thickness of 1 nm. Upon degradation, the released nontoxic byproducts, such as magnesium ions, lithium ions, and orthosilicic acid, have been identified with various bioactivities.[35−37] Therefore, it has been reported that this type of SNs can promote osteogenic differentiation of human mesenchymal stem cells (hMSCs), even in the absence of growth factors.[35−37]

By applying this multifunctional hydrogel coating on bone implants, it is expected that the resulting coated implants could show enhanced adhesion due to the strong binding interactions between catechol motifs and Ti surfaces, and present potent antimicrobial activity due to the incorporation of AMP. This coating layer should exhibit enhanced cell adhesion due to the existence of RGD motifs in the gelatin backbone, and improved osteogenesis because of the presence of SNs. Compared to conventional growth factors [e.g., bone morphogenetic protein 2 (BMP-2)], SNs have much higher biostability and lower cost.[37] AMP HHC-36 has presented potent antimicrobial activity with low resistance, along with no side effect of inhibited bone formation; these make HHC-36 very attractive for implants where osteointegration is critical.[8,10,11] In this study, we expect that the combination of SNs, HHC-36, and catechol-modified GelMA will lead to the easy production of a multifunctional implant surface with unique antimicrobial, osteogenic, and adhesive properties. In vitro physical characterization and adhesion tests were performed to validate the strong binding between the hydrogel coating and the Ti implant surface. In addition, the antimicrobial activity and cytotoxicity of the coating hydrogel, as well as the induction of hMSCs toward osteogenic differentiation, were tested in vitro.

2. MATERIALS AND METHODS

2.1. Materials. Type-A gelatin from porcine skin (300 bloom), methacrylic anhydride (94%), 2-hydroxy-1-[4-(2-hydroxyethoxy)-phenyl]-2-methyl-1-propanone (Irgacure 2959, 98%), bovine serum albumin (BSA, 98%), dimethyl sulfoxide (DMSO, 99%), succinic anhydride (99%), triethylamine (99%), 2-(N-morpholino)-ethanesulfonic acid hemisodium salt (MES, 98%), ammonium hydroxide (28%−30%), acetic acid (99.7%), N-(3-(dimethylamino)-propyl)-N′-ethylcarbodiimide hydrochloride (EDC, 98%), N-hydroxysuccinimide (NHS, 98%), dopamine hydrochloride (98%), hydrochloric acid (36.5%), Triton X-100 (BioXtra), deuterium oxide (D$_2$O, 99.9% in D), sodium hydroxide (NaOH, 98%), β-glycerol phosphate (99%), L-ascorbic acid (99%), Alizarin Red S (certified by the Biological Stain Commission), and dexamethasone (97%) were purchased from Sigma-Aldrich (St. Louis, MO). Type II collagenase was purchased from Worthington Biochemical Cor. (Lakewood, NJ). Paraformaldehyde (16% aqueous solution) was obtained from EMS (Hatfield, PA). AMP HHC-36 was purchased from CPC Scientific (Sunnyvale, CA).

Fetal bovine serum (FBS), Live/Dead Viability/Cytotoxicity Kit, PrestoBlue Cell Viability Reagent, Alexa Fluor 594−phalloidin, 4′,6-

diamidino-2-phenylindole (DAPI), α minimum essential medium (α-MEM), phosphate-buffered saline (PBS), 2-[4-(2-hydroxyethyl)-piperazin-1-yl]ethanesulfonic acid (HEPES buffer, 25 mM, pH 7.4), trypsin−ethylenediaminetetraacetic acid (trypsin−EDTA), L-glutamine, and antibiotics (penicillin/streptomycin) were purchased from Thermo Fisher Scientific (Waltham, MA). hMSCs (PT-2501) and Poietics MSCGM BulletKit were purchased from Lonza (Basel, Switzerland). *Pseudomonas aeruginosa* (*P. aeruginosa*, ATCC H1001:luxCDABE), *Escherichia coli* (*E. coli*, ATCC 252922), *Staphylococcus aureus* (*S. aureus*, ATCC 25923), *Staphylococcus epidermidis* (*S. epidermidis*, ATCC 12228) bacteria, Basal Medium 2 (BM2), and Mueller Hinton Broth (MHB) were obtained from ATCC (Manassas, VA).

2.2. Synthesis of GelMA-COOH. GelMA with a high degree of functionalization (∼90%) was prepared according to the previously reported procedure.[34,38] Purified GelMA (2.0 g) was then fully dissolved in 40 mL of PBS at 50 °C with magnetic stirring, followed by the addition of triethylamine (1.0 mL) and a solution of succinic anhydride (1.0 g) dissolved in 20 mL of dimethyl sulfoxide (DMSO). The resulting mixture was stirred overnight at 50 °C, diluted with 100 mL of PBS, neutralized by 0.1 M HCl, and dialyzed against deionized water using 3.5 kDa cutoff dialysis tubing for 1 week at room temperature to remove the impurities. The solution was lyophilized to generate GelMA-COOH as a white foam (typical yield ∼ 80%).

2.3. Synthesis and Characterization of GelMA-DOPA. To conjugate with the catechol motifs, GelMA-COOH (1.0 g) was dissolved in 10 mL of MES buffer (50 mM, pH 5). The solution was degassed by bubbling N_2 for 15 min, followed by the addition of EDC (0.20 g), NHS (0.30 g), and dopamine hydrochloride (0.20 g). Under the protection of N_2, the resulting mixture was stirred overnight at 25 °C. The solution was dialyzed against 0.01 M HCl in deionized water using 3.5 kDa cutoff dialysis tubing for 4 days, neutralized by 0.01 M NaOH, and lyophilized to generate GelMA-DOPA polymer as a white foam (typical yield ∼ 70%). The proton nuclear magnetic resonance (^{1}H NMR) spectrum was used to confirm the successful conjugation of the catechol motifs to GelMA. The degree of catechol motif functionalization was determined using UV spectrophotometry.

2.3.1. ^{1}H NMR Tests. ^{1}H NMR spectra of GelMA, GelMA-COOH, and GelMA-DOPA polymers were obtained in D_2O (99.9% D, Cambridge Isotope Laboratories, Inc., Tewksbury, MA) at a concentration of 2% (w/v) using a Varian Mercury 300 MHz NMR spectrometer. All ^{1}H NMR spectra were referenced to the peak of residual proton impurities in D_2O at $\delta = 4.75$ ppm. The NMR data were processed using ACDLABS 12.0 software (Academic Edition).

2.3.2. Determination of Catechol Content by UV Spectrophotometry. A series of dopamine hydrochloride solutions in deionized water were prepared with concentrations ranging from 0.05 to 0.5 mM as the standard solutions to obtain the working curve. The synthesized GelMA-DOPA polymer was dissolved in 50 mM MES buffer at 2.0 mg/mL to prepare the sample solutions. UV−vis absorption spectra of the solutions were measured between 200 and 400 nm. Absorbance values at 280 nm were plotted against concentrations of dopamine hydrochloride solutions to set up the working curve. Absorbance of the sample solution at 280 nm was compared to the working curve to calculate the content of catechol motifs.

2.4. UV Cross-Linking and Characterization of GelMA-DOPA Hydrogels. GelMA-DOPA polymer was dissolved in PBS at different concentrations [5−20% (w/v)]. Irgacure 2959 was added to the solution at 0.5% (w/v) as the photoinitiator. Photo-cross-linked GelMA-DOPA hydrogels were formed by pipetting a certain amount of the prepolymer solution into the desired mold or on the surface of glass slides and exposing it to 6.9 mW/cm^2 UV light (360−480 nm) for 60 s. Composite hydrogels with the addition of SNs and/or AMP were fabricated similarly with solutions containing both the photoinitiator [0.5% (w/v)] and the additives at desired concentrations.

2.4.1. Swelling Analysis. Swelling ratios of GelMA-DOPA hydrogels were evaluated at 37 °C in PBS following previously reported procedures.[39] To prepare GelMA-DOPA hydrogels for swelling ratio tests, 50 μL of prepolymer solution was first transferred into a custom-made polydimethylsiloxane (PDMS) mold with a diameter of 8 mm

and a depth of 1 mm. A glass coverslip was used to cover the mold before irradiation by UV light for 60 s. Hydrogel samples [5−20% (w/v)] were removed from the mold and coverslip, soaked in PBS, and incubated at 37 °C for 24 h to reach the equilibrium swelling state. The swollen hydrogel samples were weighed and then lyophilized to record their dry weights. The swelling ratios of hydrogel samples of 5−20% (w/v) concentrations were then calculated as the ratio of the mass increase after swelling to the mass of dried samples.

2.4.2. In Vitro Degradation Tests. Hydrogel samples for degradation tests were prepared in a manner similar to that for swelling ratio measurements. The as-prepared samples were soaked in PBS at 37 °C for 24 h to reach the equilibrium swelling state and then were weighed to record their initial masses. The GelMA-DOPA hydrogel samples of 5−20% (w/v) concentrations were kept in type II collagenase PBS solutions (2 U/mL) at 37 °C with mild shaking, and the remaining masses were regularly recorded at different time points (days 7, 14, and 21) to track the degradation kinetics.

2.5. Mechanical Characterizations. *2.5.1. Compression Tests.* Cylindrical cross-linked samples were prepared (10 mm in diameter, 2 mm in height) and incubated at 37 °C in PBS for 24 h. The GelMA-DOPA hydrogel samples of 5−20% (w/v) concentrations were then compressed at a rate of 1 mm/min using an Instron 5542 mechanical tester. Compressive moduli of the samples were determined as the slope in the linear region corresponding to 0−10% strain.

2.5.2. Lap Shear Tests. The adhesive properties of hydrogels were analyzed using an ASTM standard lap shear test (F2255-05) with modifications. Briefly, 20 μL of the prepolymer solution was applied to a glass slide pretreated with 3-(trimethoxysilyl)propyl methacrylate (TMSPMA). A Ti slide or a second TMSPMA-treated glass slide was put into contact with the hydrogel to result in an overlapping (adhesive bonded) area of around 2.0 × 2.0 cm^2. After UV light irradiation for 60 s (6.9 mW/cm^2), the samples were immersed in PBS for 2 h and then immediately strained under wet conditions until failure in a lap shear setup using an Instron 5542 mechanical tester equipped with a 100 N load cell at a cross-head speed of 1.3 mm/min. To examine the hydrogel residue on Ti substrates after breaking, a rhodamine dye was added to the prepolymer solution as a fluorescent indicator.

2.6. In Vitro Cell Culture. hMSCs were cultured in a 5% CO_2 humidified incubator at 37 °C in normal growth media (Poietics MSCGM BulletKit). Only cells before passage 5 were used for all the experiments. The osteoconductive medium was supplemented with β-glycerol phosphate and L-ascorbic acid, and the osteoinductive medium was supplemented with β-glycerol phosphate, ascorbic acid, and dexamethasone to induce osteogenic differentiation of hMSCs. The cells were passaged approximately 1 time per week and the culture medium was changed every 2 days. The cells were trypsinized, resuspended, and seeded on hydrogel-coated Ti slides placed in a 24-well plate at a density of 50 000 cells per well.

2.6.1. Cell Viability. Cell viability was determined using a live/dead assay kit following the manufacturer's instructions. Briefly, the cells were stained with calcein AM (0.5 μL/mL) and ethidium homodimer-1 (EthD-1, 2 μL/mL) in PBS for live and dead cells, respectively. The cells were incubated at 37 °C for 20 min and thoroughly washed with PBS three times. The stained cells were imaged using an inverted fluorescence microscope (Nikon TE 2000-U, Nikon instruments Inc.). The numbers of live and dead cells were counted using ImageJ software from at least three images from different areas of three samples for each experimental condition. Cell viability was calculated as the number of live cells divided by the total cell number.

2.6.2. Cell Adhesion, Proliferation, and Spreading. 4′,6-Diamidino-2-phenylindole (DAPI) and Alexa Fluor 594−phalloidin were used to stain the cells to investigate the attachment and spreading of cells on the hydrogel surfaces. Cells seeded on different substrates were fixed in 4% (v/v) paraformaldehyde for 30 min, followed by treatment with a 0.1% (w/v) Triton X-100 solution in PBS for 20 min to increase permeability and with a 1% (w/v) BSA solution in PBS for 1 h to block nonspecific binding sites. The cells were then incubated in a 1:40 dilution of Alexa Fluor 594−phalloidin in 0.1% (w/v) BSA for 45 min to stain the actin cytoskeleton and then incubated at 37 °C in a
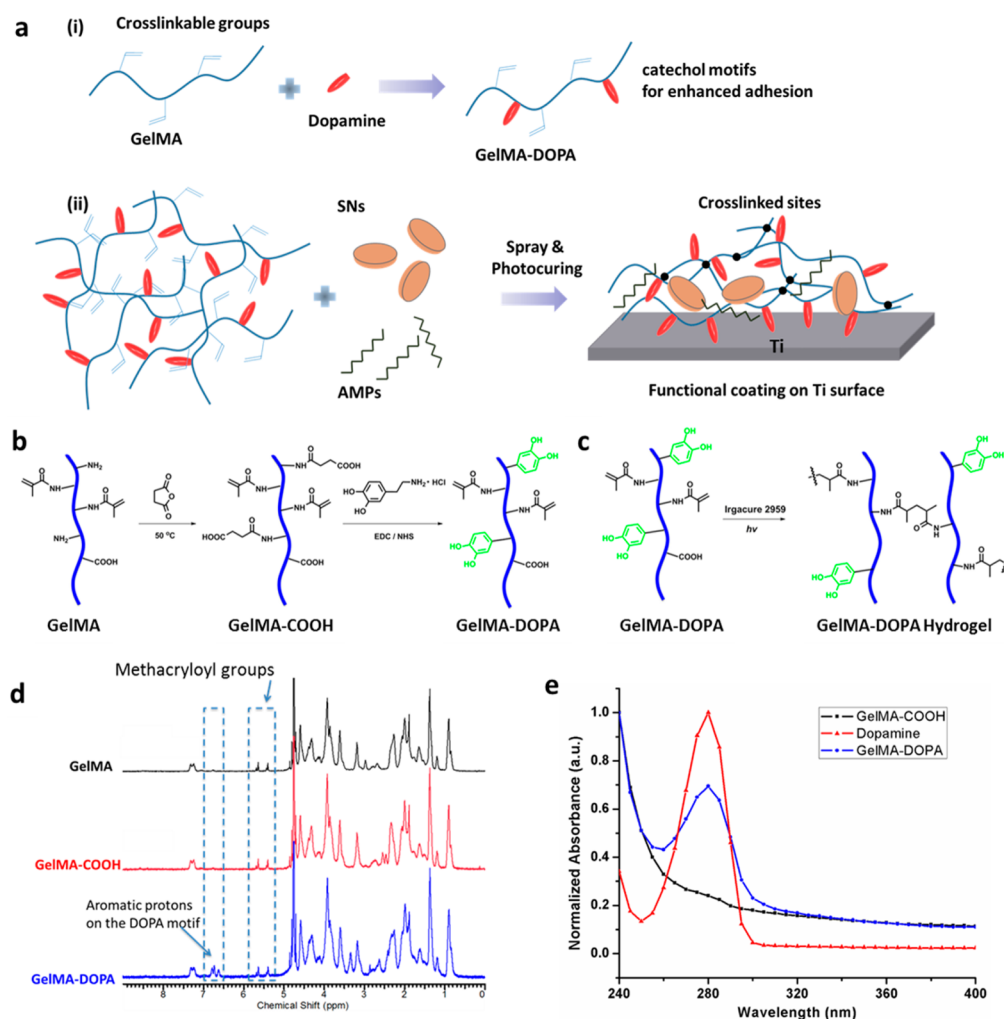
Figure 1. Synthesis and molecular characterization of the catechol-functionalized GelMA-DOPA hydrogel. (a) Schematic illustration of the formation of a highly adhesive, multifunctional hydrogel coating on Ti surfaces: (i) GelMA was modified with dopamine to introduce the catechol motifs that bind strongly to Ti and (ii) the hydrogel prepolymer solution was then mixed with the bioactive AMP and SNs, sprayed onto implant surface, and photocured in situ to form an antimicrobial and osteoinductive hydrogel coating layer. (b) Synthetic scheme of dopamine-containing GelMA (GelMA-DOPA). (c) Formation of a cross-linked network with dangling dopamine motifs upon UV exposure in the presence of a photoinitiator. (d) ^{1}H NMR spectra of GelMA, GelMA-COOH, and GelMA-DOPA. Comparison indicated the appearance of additional resonance peaks in the aromatic region of the GelMA-DOPA spectrum, which can be assigned to the DOPA motifs. (e) UV−vis absorption spectra of GelMA-COOH, dopamine hydrochloride, and GelMA-DOPA. Appearance of the peak centered at 280 nm indicated successful conjugation of the DOPA motifs.

0.1% (w/v) DAPI solution in PBS for 10 min to stain the cell nuclei. After each staining step, the samples were carefully washed with PBS three times before visualizing with a Nikon TE 2000-U microscope. ImageJ software was used to count the number of DAPI-stained nuclei.

2.6.3. PCR Experiments. PCR experiments were performed to quantify the expression of genes related to osteogenesis. For quantitative PCR (qPCR) experiments, SYBR Green Real-Time PCR Master Mixes (Thermo Fisher Scientific) and primers obtained from Integrated DNA Technologies (IDT, Coralville, IA) were used [see Table S1 in the Supporting Information (SI)].

2.6.4. Alizarin Red S Staining. Cells were fixed with 10% formalin for 20 min and then thoroughly washed with PBS and deionized (DI) water, before the addition of a 2% (w/v) solution of Alizarin Red S with pH 4.2. After 10 min of incubation at 37 °C, the samples were washed with DI water for microscope imaging. To quantify the coloration after staining, 10% (v/v) acetic acid was added to the cells and incubated overnight. After that, the resulting mixture was centrifuged for 15 min at 20 000g and the supernatant was collected and neutralized with 10% (v/v) ammonium hydroxide. The absorption

value at 405 nm of the solutions was recorded using a microplate reader.

2.7. Release Profile of AMP HHC-36. In vitro release profile of AMP loaded within 20% (w/v) GelMA-DOPA hydrogels was obtained by using ultraviolet−visible (UV−vis) spectroscopy. The absorptions at 280 nm, known as the characteristic absorption peak for tryptophan residues, were recorded to monitor the concentration of released AMP in solutions. The hydrogel specimens were prepared in triplicate by coating on a Ti substrate and then immersed in 1 mL of PBS in a glass vial with rotation at 37 °C. At designed time points, 500 μL of the solution was removed from the vial with fresh PBS replenishing the volume. Absorptions at 280 nm of the sample solutions were measured to determine the cumulative release ratio of AMP. A series of standard solutions of AMP in the concentration range from 1 to 128 μg/mL in deionized water were prepared to obtain the working curve. Quantification of AMP concentration was then calculated on the basis of the external standard curve method. The release experiment was performed using GelMA-DOPA hydrogel samples without AMP loads as the blank control to eliminate the possible influence from degraded hydrogel fragments.

2.8. Antimicrobial Activity Tests. Antimicrobial activity of the AMP-loaded GelMA-DOPA hydrogels was tested against both Gram-positive (*S. aureus* and *S. epidermidis*) and Gram-negative (*P. aeruginosa* and *E. coli*) bacteria in the mid-logarithmic phase of growth. The bacterial suspensions were resuspended using MHB to reach a final cell density of 10^6 colony-forming units (cfu)/mL. To perform the survival assay, 400 μL of the bacterial suspensions were dropped onto three bare Ti plates, three GelMA-DOPA-coated Ti plates, and three GelMA-DOPA-coated Ti plates loaded with AMP (1 mg/mL), respectively, followed by rinsing with distilled water. After 4 and 24 h of incubation with *P. aeruginosa*, *E. coli*, *S. aureus*, and *S. epidermidis* bacterial suspensions, samples were taken and inoculated on nutrient agar plates and incubated overnight at 37 °C. Bacterial survival rates were assessed by counting the number of cfu. The antimicrobial activity of hydrogel samples was also confirmed by scanning electron microscopy (SEM) imaging of samples incubated with 10^6 cfu/mL of the selected bacteria overnight at 37 °C. SEM images were obtained using a FEI/Philips XL30 FEG ESEM instrument (15 kV). The substrate without an AMP-loaded GelMA-DOPA coating layer was used as control.

2.9. Statistical Analysis. For comparison, experimental data were processed using one-way ANOVA followed by Bonferroni's posthoc test (GraphPad Prism 5.02) software. Error bars represented the mean $\pm$ standard deviation (SD) of measurements ($*p < 0.05$, $**p < 0.01$, and $***p < 0.001$).

3. RESULTS AND DISCUSSION

3.1. Preparation of Photo-Cross-Linkable GelMA-DOPA. Derived from partial hydrolysis of collagen, gelatin has been widely used in tissue engineering applications, due to its biocompatibility, biodegradability, and low cost.[20,40−44] During the past few years, our group has popularized the use of a photo-cross-linkable gelatin derivative, GelMA, for various biomedical applications.[33,34,45−47] Due to the existence of RGD sequences along the gelatin backbone, GelMA hydrogels were found to support cell attachment and spreading.[15,45] To develop a sprayable coating material, adhesion properties to both implant and tissue surfaces are critical. In recent years, inspired by natural adhesives secreted by mussel species,[22,24,28,48,49] the mechanism of adhesion improvement by introduction of catechol motifs has been widely applied to design adhesives with strong binding properties to diverse surfaces, in particular wet surfaces.[22] Here, we propose to chemically conjugate GelMA polymer with dopamine (DOPA) to introduce catechol motifs and synthesize GelMA-DOPA, which could combine the regenerative properties of GelMA-based hydrogels with enhanced adhesion properties of the catechol motifs (Figure 1a).

GelMA-DOPA was prepared from GelMA via a two-step procedure, as shown in Figure 1b. First, GelMA was reacted with an excess amount of succinic anhydride to fully convert all the remaining reactive amine groups to carboxylic groups. The resulting GelMA-COOH intermediate was then allowed to react with dopamine hydrochloride via the EDC/NHS-mediated coupling reaction (Figure 1b). The resulting mixture was then purified by dialysis against deionized water and finally lyophilized to obtain a white solid. Similar to GelMA, the product GelMA-DOPA can also be cross-linked to form hydrogels by UV light exposure in the presence of a photoinitiator, as shown in Figure 1c.

^{1}H NMR data of GelMA, GelMA-COOH, and GelMA-DOPA were obtained in D_2O to confirm the successful conjugation of the catechol motifs. As shown in Figure 1d, in the ^{1}H NMR spectrum of GelMA-DOPA (blue line), additional peaks in the aromatic region appeared after the EDC/NHS

coupling reaction that were not observed in the spectra of either GelMA (black line) or GelMA-COOH (red line). These peaks are characteristic of the catechol motifs according to previous reports.[50,51] However, comparison of the Fourier transform infrared (FT-IR) spectra among GelMA, GelMA-COOH, and GelMA-DOPA did not result in identifiable differences to reflect the introduction of the DOPA motifs (Figure S1, SI). This is probably due to the fact that the chemical modification did not add new functional groups that have characteristic infrared (IR) absorption peaks. In addition, there was a strong peak centered at 280 nm in the UV−vis absorption spectrum of GelMA-DOPA,[52] as shown in Figure 1e (blue line). By comparing with the spectra of dopamine hydrochloride and the precursor GelMA-COOH, it is clear that this absorption peak appeared due to the presence of the catechol motifs in GelMA-DOPA. To quantitatively determine the content of catechol motifs, the absorption values at 280 nm (A_{280}) of a series of dopamine hydrochloride solutions with different concentrations ranging from 0 to 1 mmol/mL were measured and plotted to obtain a working curve. By assuming that the conjugated catechol motifs have an identical molar extinction coefficient with the free small molecules, the content of catechol groups in GelMA-DOPA was determined as 0.5 mmol/g. This value suggested roughly 5 catechol groups per 100 amino acid residues in the backbone.

The catechol-modified photo-cross-linkable GelMA-DOPA polymer was used to design sprayable antimicrobial and osteoinductive hydrogel coatings for implants. To introduce more functions, two additional components, namely AMP and SNs, were added to GelMA-DOPA macromers to improve the antimicrobial and osteoinductive properties. It has been shown that the release of AMP from the hydrogel coating provides the antimicrobial activity[53,54] and that exposure of hMSCs to the SNs is known to induce osteogenic differentiation of hMSCs, as reported in previous publications.[37,55,56]

3.2. Physical and Adhesion Characterizations of the Engineered Hydrogels. We characterized the physical properties of GelMA-DOPA hydrogels with different formulations in terms of compressive modulus, swelling ratio, and degradation behavior. As shown in Figure 2a, the compression test illustrated an expected positive correlation between GelMA-DOPA concentrations and the compressive moduli of the resulting hydrogels, ranging from 8.0 $\pm$ 1.7 kPa for 5% (w/v) GelMA-DOPA hydrogels to 120 $\pm$ 12 kPa for 20% (w/v) hydrogels. The tunable compressive moduli of GelMA-DOPA hydrogels provide the basis for fine-tuning the properties of the hydrogel coating matrix, since it has been known that hydrogel surfaces with different compressive moduli could affect the morphology, proliferation, and differentiation of stem cells.[57,58]

Addition of SNs (100 μg/mL) and AMPs (1.0 mg/mL) at the relevant concentrations did not show significant influence on the compressive moduli of the 20% (w/v) GelMA-DOPA hydrogels (Figure 2b), which could be attributed to the low loading concentrations. These concentrations were determined from previous reports,[10,37,56] which have been shown to be the optimized concentrations of functional additives. We further analyzed the swelling ratios of GelMA-DOPA hydrogels fabricated from prepolymers of different concentrations (Figure 2c), which indicated water absorption capacity. As expected, a reverse relationship between swelling ratio and prepolymer concentration was identified, ranging from 16.3 $\pm$ 1.5 for 5% (w/v) GelMA-DOPA hydrogels to 5.5 $\pm$ 0.4 for 20% (w/v) hydrogels. When mixed with different additives, the swelling
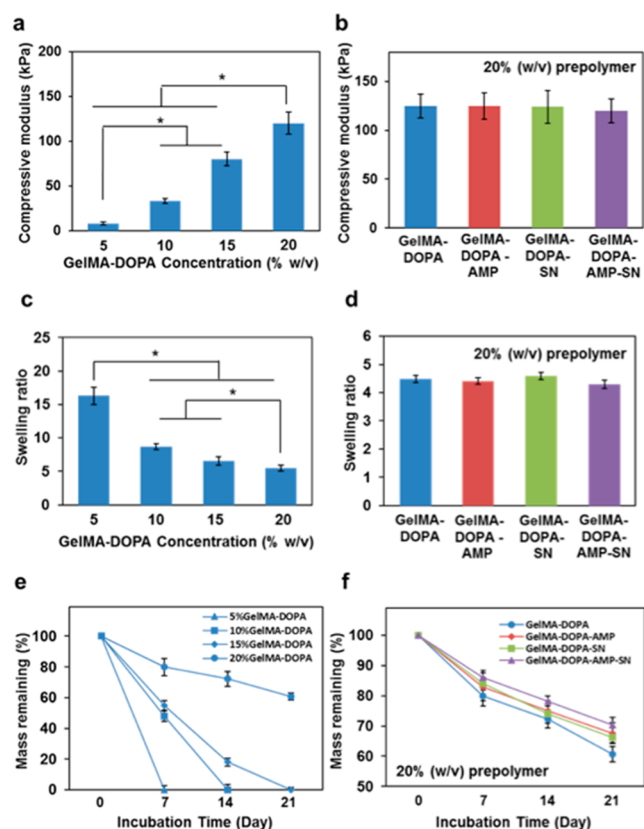
Figure 2. Physical characterizations of GelMA-DOPA hydrogels loaded with different additives. (a) Compressive moduli of GelMA-DOPA hydrogels at different prepolymer concentrations. (b) Compressive moduli of GelMA-DOPA hydrogels of 20% (w/v) prepolymer concentrations with AMP and/or SN additives. (c) Mass swelling of GelMA-DOPA hydrogels at different prepolymer concentrations. (d) Mass swelling of GelMA-DOPA hydrogels of 20% (w/v) prepolymer concentrations with AMP and/or SN additives. (e) In vitro degradation profiles of GelMA-DOPA hydrogels formed at different prepolymer concentrations. (f) Degradation profiles of different hydrogel compositions of 20% prepolymer concentration (*$p < 0.05$).

ratio of 20% (w/v) GelMA-DOPA hydrogels did not change significantly, which fell in a narrow range of around 4.5 times (Figure 2d). The relatively low swelling ratio can limit the amount of water penetration and the degree of volume change upon implantation, which is beneficial for applications as a hydrogel coating layer to metal implants.

To evaluate the degradation kinetics, GelMA-DOPA hydrogel samples were incubated in PBS solutions with collagenase (2 U/mL) at 37 °C and the remaining masses were monitored at different time points. As shown in Figure 2e,f, the degradation rates were faster for hydrogels fabricated from lower hydrogel concentrations. For 20% (w/v) GelMA-DOPA hydrogels, the remaining mass was 60–70% at day 21. In contrast, GelMA-DOPA hydrogels made from 5%–15% (w/v) prepolymer concentrations totally disappeared within 1–3 weeks. To serve as the hydrogel coating layer for Ti implants, a stability of hydrogels of up to several weeks or longer is an important parameter to ensure that the delivery of loaded components will cover the short-term (several weeks) recovery range after surgery. From these results, we selected the 20% (w/v) hydrogels to investigate the effects of bioactive component addition on the degradation kinetics. As shown in

Figure 2f, the addition of AMP and SNs to 20% (w/v) GelMA-DOPA hydrogels did not bring about significant changes in degradation rates, suggesting the possible controlled release of bioactive loadings from the hydrogel for up to several weeks.

Considering the working conditions of implants, achieving improved adhesion properties to Ti surfaces under wet environments is critical to the success of a multifunctional hydrogel coating on Ti implants. Therefore, we performed lap shear tests under swollen conditions of the hydrogel to characterize the in vitro adhesion properties of modified GelMA-DOPA based on the modified ASTM standard F2255-05 (Figure 3a). As shown in Figure 3b, we observed enhanced lap shear strengths along with increasing GelMA-DOPA concentrations, which ranged from 19.6 ± 1.9 kPa for 5% (w/v) GelMA-DOPA hydrogels to 60.7 ± 8.9 kPa for 20% (w/v) GelMA-DOPA hydrogels (Figures 3b), likely due to an increased DOPA motif content at higher prepolymer concentrations. When compared to pristine GelMA and GelMA-COOH hydrogels at the same 20% (w/v) concentration (Figure 3c), it was revealed that the adhesion strengths of GelMA-DOPA hydrogels (60.7 ± 8.9 kPa) were significantly higher than those of GelMA or GelMA-COOH hydrogels (15.2 ± 3.0 and 16.4 ± 0.3 kPa, respectively). The almost 4-fold increase in lap shear adhesion strength of GelMA-DOPA hydrogel under wet conditions could be attributed to the strong binding interactions between the catechol motifs in GelMA-DOPA hydrogels, which largely improved coating stability on Ti surfaces.[23]

The lap shear tests provided quantitative data to reflect the adhesion increase due to the introduction of catechol motifs to the hydrogel, but these values could not show the possibly different failure modes from the samples. To further understand the failure mode of hydrogel adhesives in lap shear tests, we investigated the surface morphology of the Ti substrates after adhesion failure. To qualitatively assess the amount of hydrogel residue on Ti substrates after adhesion failure in the lap shear tests, we mixed a rhodamine dye with the prepolymer solutions to serve as a fluorescent indicator. After the lap shear tests, we checked the Ti substrates under a fluorescence microscope. As shown in Figure 3di, the Ti surface coated with GelMA-DOPA was found to be still covered with dye-doped hydrogels, as compared with those coated with GelMA or GelMA-COOH. These results indicated that the failure mechanism of GelMA-DOPA hydrogel in lap shear tests is a cohesive failure due to the relatively low mechanical stiffness of the hydrogel. In contrast, for GelMA or GelMA-COOH, the breaking of adhesion is via adhesive failure due to the poor adhesion capability of the hydrogel layer to Ti surfaces. This comparison highlighted the feasibility of introducing catechol motifs to enhance hydrogel–metal adhesion.[31]

We also used SEM to observe the morphological differences of the Ti substrates after lap shear tests with different hydrogels. As shown in Figure 3dii,iii, both vertical and lateral SEM images of the Ti substrates clearly showed the rough surface of GelMA-DOPA-coated Ti plates with residue hydrogel coating due to the strong binding ability of this hydrogel. On the other hand, SEM images of GelMA- and GelMA-COOH-coated Ti substrates were relatively smooth with little hydrogel residue after lap shear tests. These results confirmed the different failure mechanisms of mussel-inspired GelMA-DOPA hydrogels and pristine GelMA without catechol motifs. Since unmodified Ti substrates were used in these tests, the increased adhesion with increasing GelMA-DOPA prepolymer concen-
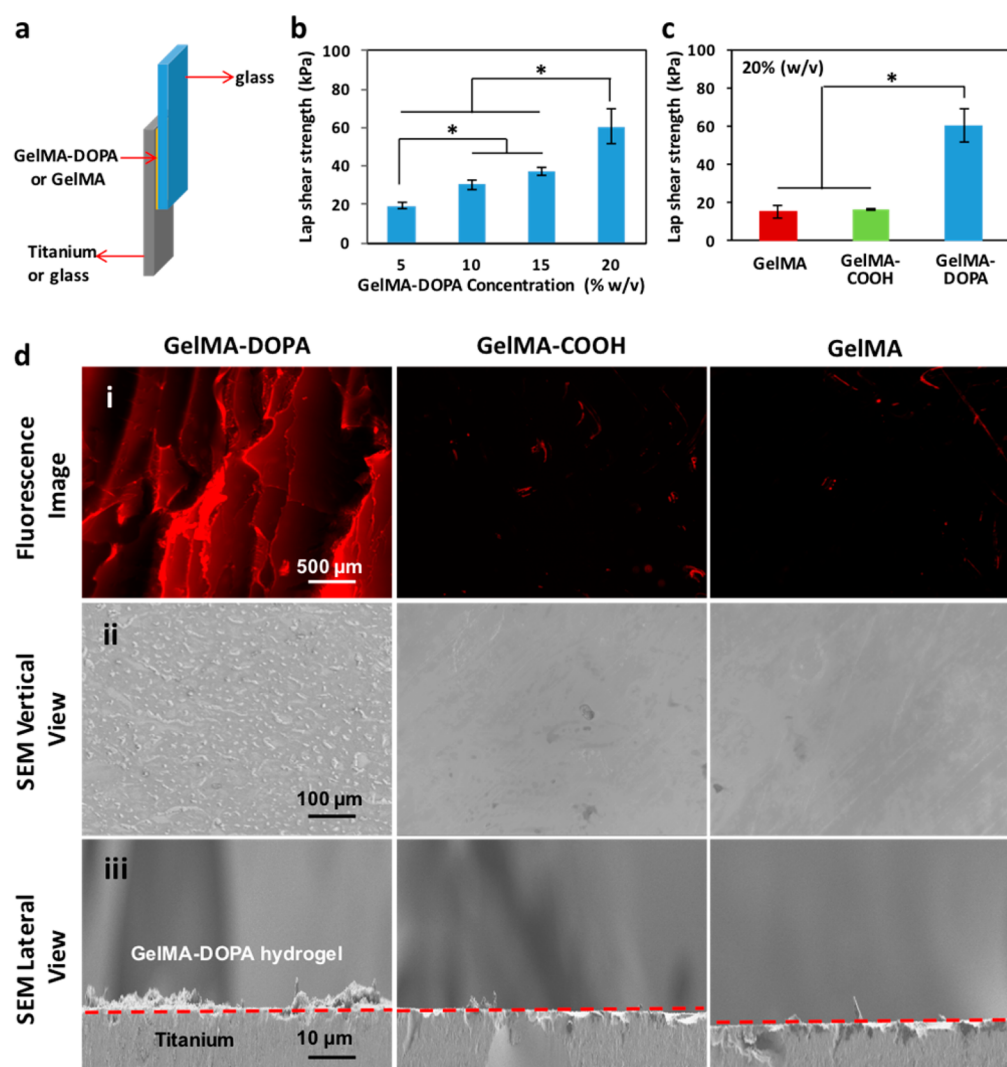
Figure 3. Adhesion properties of GelMA-DOPA hydrogels to a Ti surface. (a) Schematic illustration of the experimental setup for testing the lap shear strength. (b) Lap shear strengths of GelMA-DOPA hydrogels of different prepolymer concentrations. (c) Comparison of lap shear strengths obtained from GelMA, GelMA-COOH, and GelMA-DOPA hydrogels of 20% (w/v) prepolymer concentration ($*p < 0.05$). (d) Evaluation of Ti surfaces coated with different hydrogels after adhesion breaking in lap shear tests: (i) representative fluorescent images of Ti surfaces coated with hydrogels mixed with a rhodamine dye and representative SEM images of titanium surfaces from (ii) vertical and (iii) lateral views.

trations was related to the higher content of catechol motifs, which provided stronger adhesion. This is different from other studies where surface topology factors or surface energy differences of the Ti substrate play a role in improved adhesion properties.[59] It is also suggested that the adhesion properties of catechol-containing hydrogels to Ti surfaces might be further improved by increasing the cohesive strengths of the matrix hydrogels by known strategies, such as formulating hybrid hydrogels[60] or interpenetrated hydrogel networks.[61]

From these results, it was revealed that, in general, the swelling ratio was inversely correlated with GelMA-DOPA prepolymer concentrations, while compressive modulus and lap shear strength were positively correlated with prepolymer concentrations. Lower prepolymer concentrations typically resulted in lower cross-linking density and formation of hydrogels with lower mechanical properties. This is consistent with previous studies on GelMA hydrogels where the modulus was reduced over 10-fold when the polymer concentration decreased from 20% (w/v) to 5% (w/v).[34] For GelMA-DOPA samples, since the adhesion failure model is cohesive failure

(hydrogel breaking), lower mechanical strengths lead to lower lap shear strengths. Therefore, the hydrogel with lower stiffness exhibited lower shear adhesion. Our results provide understanding toward the rationale design of hydrogel coatings with better performances.

3.3. Release Profile of AMP from GelMA-DOPA Hydrogels. To incorporate antimicrobial activity to the sprayable and photo-cross-linkable hydrogel coating material, a broad-spectrum AMP HHC-36 was added in the prepolymer solution. The AMP HHC-36 has a sequence of KRWW-KWWRR and has previously been loaded in calcium phosphate and vertically aligned TiO_2 nanotube coatings on Ti surfaces to inhibit microbe growth.[8−11] It was demonstrated that these positively charged short peptides could show high binding affinity toward the negatively charged bacteria membrane through electrostatic interactions, thus promoting the targeting and antimicrobial capability.[62] Importantly, the HHC-36 peptide showed no inhibition of new bone formation, making it suitable as an additive for loading on Ti implants where osteointegration after implantation is important.[8,10,11] To

monitor the release profile of AMP HHC-36 from the cross-linked GelMA-DOPA hydrogel, 1 mg/mL AMP was mixed with 20% (w/v) GelMA-DOPA prepolymer solutions containing 0.5% (w/v) photoinitiator.[8,10] To achieve this, 20 μL of the mixed solution was drop-coated on a glass slide and cured under 6.9 mW/cm^2 UV light (360−480 nm) for 60 s to form the cross-linked hydrogel coating layer. The prepared samples were incubated at 37 °C in PBS. The amount of AMP released from GelMA-DOPA hydrogel was determined by measuring the absorption at 280 nm (Figure S2a, SI). Pristine GelMA-DOPA hydrogel samples with no AMP loading were used as the blank control.

A burst release of AMP was observed to reach a cumulative release of 37% within the first 24 h after incubation (Figure S2b, SI). After that, a relatively steady release of AMP was observed for the next 20 days of incubation, resulting in an increase of cumulative release to roughly 90%. Previous reports on the release of AMP loaded in a calcium phosphate coating or TiO$_2$ nanotubes indicated much faster release kinetics, which reached the maximum cumulative release amount within a few hours.[8,10] Steady sustained release of the antimicrobial components could be achieved from a multilayered coating that combined three layers of TiO$_2$ nanotubes, calcium phosphate, and a phospholipid film but required a complicated fabrication process.[10] Due to the lack of conjugation between AMP and the hydrogel matrix, we reason that the release mechanism was diffusion-controlled. Indeed, the release of AMP was accelerated in the presence of collagenase (Figure S2b, SI). The prolonged release of AMP from the GelMA-DOPA hydrogel coating layer is believed to be a critical criterion to achieve protection against implant-associated infections for the first few weeks after surgery. Moreover, in cases where long-term delivery of AMP is required, this material design also allows easy surface immobilization of AMPs through copolymerization during the photo-cross-linking. Therefore, we believe that our approach provides a suitable method for controlled release of AMP from Ti implant surfaces.

3.4. Antimicrobial Activity of AMP-Loaded GelMA-DOPA Hydrogels.

The antimicrobial capability of the released AMP was first tested using the cfu assay. Two experimental groups, GelMA-DOPA−AMP and GelMA-DOPA−AMP−SN, were tested with blank GelMA-DOPA hydrogels as the control. Both representative Gram-positive bacteria (S. aureus and S. epidermidis) and Gram-negative bacteria (P. aeruginosa and E. coli) were used to assess the antimicrobial activity of the AMP-loaded hydrogels by the cfu counting method.[10] After 4 and 24 h of incubation, the cfu values were measured and compared to the initial dose. For all four different bacteria used in the test, the control samples showed significant increases of cfu values during incubation, as expected. In contrast, AMP-loaded hydrogels demonstrated excellent antimicrobial activity, since significant reduction (several orders of magnitude) in cfu values was observed at 4 h and complete elimination of bacteria was noted at 24 h (Figure 4a−d). The bactericidal effect was most profound against S. epidermidis, which showed the lowest cfu value after 4 h. Moreover, the antimicrobial activity was not significantly influenced by the addition of SNs. Considering the high initial numbers of bacteria ($\sim$10^6−10^8 cfu/mL), it is suggested that the loading of AMP in the GelMA-DOPA hydrogel coating will be efficient in clinical circumstances, where the actual numbers of bacteria encountered could be much lower.[6]
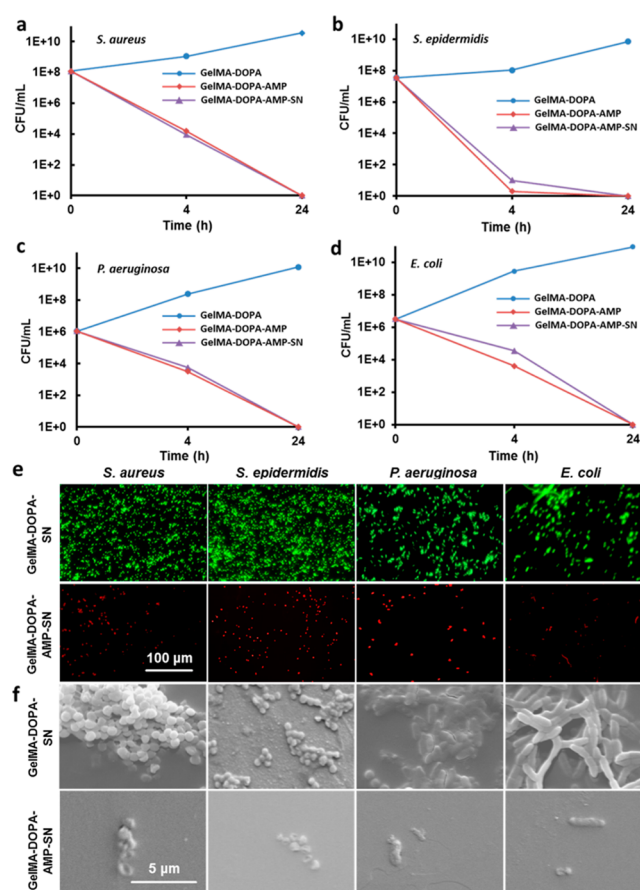

Figure 4. Antimicrobial activity of GelMA-DOPA hydrogels at 20% (w/v) prepolymer concentration with AMP and/or SN additives. Bacteria colony count experiments against different bacteria: (a) S. aureus, (b) S. epidermidis, (c) P. aeruginosa, and (d) E. coli, seeded on different hydrogel formulations at 20% (w/v) concentration. Changes in cfu at 4 and 24 h after incubation were taken as the measure of antimicrobial ability. Error bars in parts a−d are too small to present proportionally in the panels. (e) AMP released from GelMA-DOPA−AMP−SN samples demonstrated efficient antimicrobial ability to kill the tested bacteria, S. aureus, S. epidermidis, P. aeruginosa, and E. coli. Compared to GelMA-DOPA−SN samples without AMP loading, no live bacteria were observed on the GelMA-DOPA−AMP−SN samples after 24 h culture (green, live bacteria; red, dead bacteria; scale bar, 100 μm). (f) SEM images showing surfaces of GelMA-DOPA−SN and GelMA-DOPA−AMP−SN hydrogels incubated overnight with S. aureus, S. epidermidis, P. aeruginosa, and E. coli. Very few bacteria were observed on the AMP-loaded samples (scale bar, 5 μm).

The antimicrobial activity was also evaluated by staining the bacteria using a live/dead assay. Four different bacteria were seeded on the surface of hydrogel coatings and cultured for 24 h before staining. The viability of the bacteria was monitored by measuring their membrane integrity. The green-fluorescent nucleic acid dye is able to penetrate the cell membrane of both healthy and dead bacteria cells, while the red-fluorescent propidium iodide dye penetrates only damaged membranes and quenches the green fluorescence in dead cells.[63] As a result, this staining can provide direct, visualized identification and differentiation between living and dead bacteria cells. As shown in Figure 4e, bacteria cultured with GelMA-DOPA−AMP−SN hydrogels were found to have very low viability after 24 h, in contrast with the results from the GelMA-DOPA−SN formulation, which showed high cell viability for all four species

of bacteria. Similarly, the assay results for bacteria cultured on GelMA-DOPA−AMP and GelMA-DOPA hydrogels also showed low viability and high viability, respectively (Figure S3a, SI). Therefore, the significant changes in bacteria viability were thus attributed to the release of AMP from the hydrogels.

Inhibition of biofilm formation is also a critical requirement to prevent implant-associated infections, since bacteria attached to biofilms demonstrate enhanced resistance to antibiotics.[4] SEM images of the control GelMA-DOPA−SN (Figure 4f, top panels) and GelMA-DOPA (Figure S3b, top panels, SI) hydrogel surfaces with seeded bacteria showed that the bacteria could adhere to the surface and form cell aggregates with different morphologies after 48 h of incubation. Under similar conditions, however, only very few bacteria were able to adhere to the GelMA-DOPA−AMP−SN (Figure 4f, bottom panels) and GelMA-DOPA−AMP (Figure S3b, bottom panels, SI) hydrogel surfaces, thus preventing biofilm formation over the surface. The ability of AMP-loading GelMA-DOPA hydrogels to prevent biofilm formation is an important aspect in clinical applications, where the removal of biofilm after its buildup is almost impossible.[64] From the results of controlled release tests of AMP from the hydrogel coating and the antimicrobial activity tests, it was confirmed that the AMP-loaded GelMA-DOPA hydrogels were able to reduce bacterial growth and accumulation on the Ti implants, which is promising to address infection-associated implant failures.

3.5. Cytotoxicity Tests of GelMA-DOPA Hydrogels.
Cytotoxicity of the implant-coating hydrogels was evaluated by 2D culture of hMSCs on hydrogel surfaces with different formulations. Since the hydrogel coating formulation is based on a gelatin derivative, it is expected that cells could adhere to the hydrogel coating surface and show spreading morphology due to the existence of cell-adhesive motifs in the gelatin backbone.[34,45,65] The cells were seeded on the hydrogel surfaces and cultured for 7 days. Cell viability was examined by the live/dead staining at days 1, 3, and 7 of culture. As shown in Figures 5a,c and S4a (SI), in general, high viability (>90%) of the cells was observed for all the experimental conditions, suggesting that this implant coating hydrogel was cytocompatible. Moreover, the addition of AMP and SNs in the hydrogel at the doping concentrations did not reduce the high cytocompatibility of the GelMA-DOPA-based hydrogels, which is consistent with previous results.[9,10,37,56]

The ability of the hydrogel surface to support cell spreading was validated by the staining of f-actin filaments and nuclei of the cells [Figures 5b and S4b (SI)]. In addition, quantification of the number of cell nuclei in a unit surface area (Figure 5d) indicated that hMSCs seeded on the hydrogel surfaces were able to proliferate along with increasing culture time. From counting the nuclei per unit area, the cell density of hMSCs seeded on various GelMA-DOPA hydrogels increased almost 5-fold at day 7 compared with that at day 1. These results confirmed that the presence of cell-binding motifs when using gelatin-based materials could support cell spreading and cellular growth in vitro.[34]

We also used the Prestoblue assay to monitor the metabolic activity of the seeded cells. The corrected absorbance difference of the assay solution between 570 and 600 nm after culturing with cells for 2 h was an indicator of the total metabolic activity of cells. As shown in Figure 5e, from day 1 to day 7, over a 3-fold increase in absorbance difference was detected, reinforcing the conclusion that the hydrogel formulations were not cytotoxic to hMSCs in in vitro cell culture.
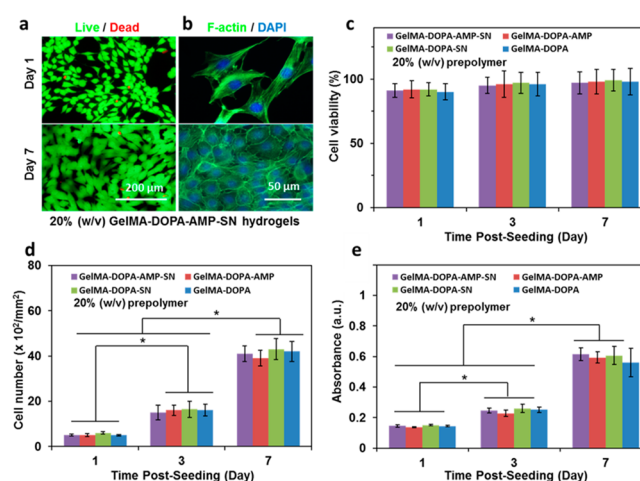

Figure 5. In vitro cytotoxicity of different hydrogel formulations at 20% (w/v) prepolymer concentration. (a) Representative live/dead staining images of hMSCs seeded on the surface of GelMA-DOPA−AMP−SN hydrogels on days 1 and 7 (scale bar, 200 μm). (b) Representative microscopic images of hMSCs seeded on the surface of GelMA-DOPA−AMP−SN hydrogels with staining for f-actin/cell nuclei on days 1 and 7 (scale bar, 50 μm). (c) Quantification of cell viabilities at 1, 3, and 7 days after cell seeding on different hydrogel surfaces. (d) Quantification of cell densities measured as the number of DAPI-stained nuclei per unit area at 1, 3, and 7 days after cell seeding on different hydrogel surfaces. (e) Corrected absorbance difference between 570 and 600 nm obtained from the Prestoblue assay at 1, 3, and 7 days after cell culture (*$p < 0.05$).

3.6. Enhanced Osteogenesis of hMSCs.
It has been reported that the SNs could induce osteogenic differentiation of stem cells including hMSCs, even in the absence of any external osteoinductive factors.[37,56] As a result, when SNs are loaded in the spray formulation for implants, it is expected that the effects of osteogenesis induction could be used to improve integration with the surrounding tissues and enhance new bone formation.[7,15,66,67] To validate this assumption, hMSCs seeded on different hydrogel surfaces were cultured in an osteogenic medium (100 nM dexamethasone, 10 mM β-glycerol phosphate, and 50 μg/mL ascorbic acid). The expressions of several representative osteogenic biomarkers were monitored using qPCR, such as the early osteogenic marker alkaline phosphatase (ALP), osteo-related proteins osteocalcin (OCN) and osteopontin (OPN), and Runt-related transcription factor 2 (RUNX2), which is a member of the RUNX transcription factor family and expressed in mineralized tissues.[68,69] Upregulation of these biomarkers is correlated with enhanced osteogenic differentiation of hMSCs. As shown in Figure 6, qPCR results suggested that, when loaded with SNs, significantly enhanced expressions of ALP, OCN, OPN, and RUNX2 were observed at day 28. Moreover, the levels of protein expression did not significantly differ by introduction of AMP in the hydrogels, which is consistent with previous studies on AMP, making it suitable for the design of a multifunctional implant-coating hydrogel.[8]

The degree of mineralization of hMSCs cultured on hydrogel surfaces was analyzed by using Alizarin Red S staining for the inorganic calcium deposition,[37] which is a characteristic indicator of the formation of bonelike structures as a result of osteogenic differentiation (Figure 7a). Compared to hydrogels without SN loadings, hMSCs cultured in the presence of SNs showed significantly enhanced production of extracellular
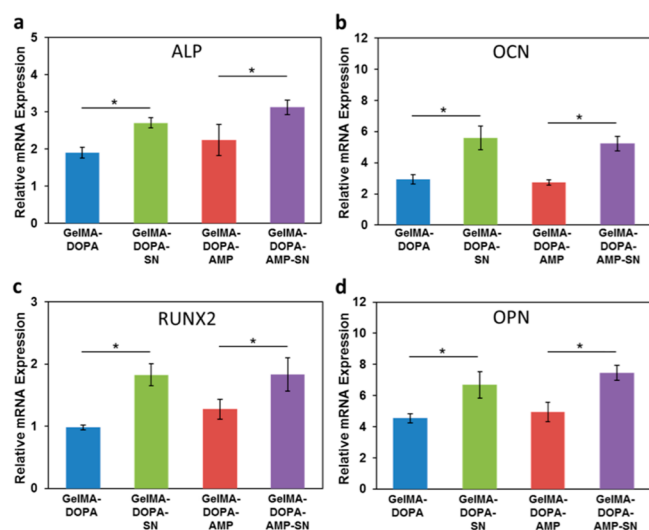
Figure 6. Effects of GelMA-DOPA hydrogels loaded with AMP and/or SN additives at 20% (w/v) prepolymer concentration on osteogenic differentiation of hMSCs. Enhanced osteogenesis was measured by qPCR quantification of relative mRNA expressions of osteogenic biomarkers: (a) ALP, (b) OCN, (c) OPN, and (d) RUNX2 at day 28 after incubation (*$p < 0.05$).
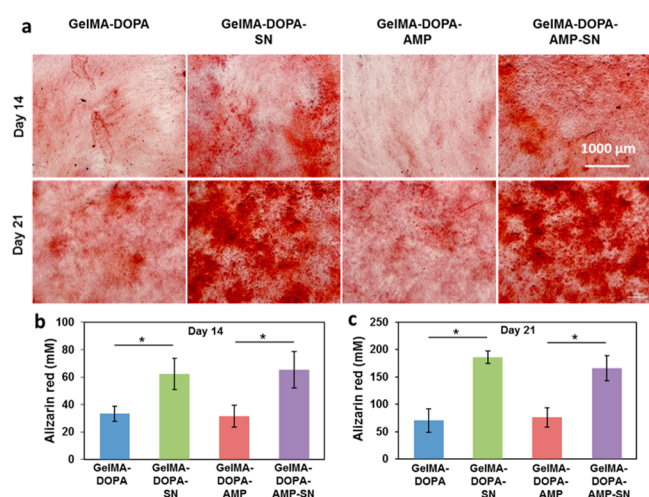

Figure 7. Effects of GelMA-DOPA hydrogels loaded with AMP and/or SN additives at 20% (w/v) prepolymer concentration on mineralized extracellular matrix production. (a) Quantitative analyses of mineralized extracellular matrix production in hMSCs were measured by the Alizarin Red S staining on days 14 and 21 of culture. Quantification of the amount of Alizarin Red stain on (b) day 14 and (c) day 21 (*$p < 0.05$).

matrix mineralization on both days 14 and 21 (Figures 7b,c). The increased mineralization was attributed to the bioactivity of SNs to promote osteogenic differentiation of hMSCs, which confirmed that when loaded in GelMA-DOPA hydrogels, the SNs could still induce mineral deposition of hMSCs in vitro.[56] These in vitro results indicated the potential to promote osteointegration when implanted in vivo.[1,18,70]

4. CONCLUSION

In this study, we reported the design and evaluation of a mussel-inspired multifunctional coating hydrogel for Ti implants to prevent infection and to promote osteogenesis of hMSCs. First, GelMA-DOPA was prepared by chemically conjugating catechol motifs to GelMA via EDC/NHS chemistry to improve the adhesion of the hydrogel coating to Ti surfaces. After spray-coating onto the implant surface, photo-cross-linking was used to readily form the hydrogel coating. Enhanced adhesion of the hydrogel to Ti surfaces was observed as a result of the catechol motifs. Moreover, two additional active components, AMP HHC-36 and SNs, were loaded into the prepolymer solution to introduce the antimicrobial activity and the ability to induce osteogenesis. Prolonged release of AMP from the hydrogel was monitored to last for 21 days, which efficiently ablated four different species of representative bacteria and thus prevented the formation of biofilms on the surfaces. In addition, the hydrogel formulations were found to be compatible with hMSCs and able to support cell adhesion, spreading, and proliferation in 2D culture models. Importantly, hMSCs cultured on SN-loaded hydrogels demonstrated enhanced osteogenic differentiation, as confirmed by upregulated expressions of several osteo-related biomarkers revealed by qPCR and increased extracellular matrix mineralization revealed by the Alizarin Red S staining. These in vitro results suggested that this GelMA-DOPA-based implant spray can provide a promising alternative method to design a multifunctional hydrogel coating for Ti implants with sought after properties, including supporting cell adhesion, spreading and growth; preventing implant-associated infections; and enhancing implant integration with surrounding tissues by promoting osteogenesis of stem cells.

■ ASSOCIATED CONTENT

Ⓢ Supporting Information

The Supporting Information is available free of charge on the ACS Publications website at DOI: 10.1021/acsami.6b16779.

> FT-IR spectra of GelMA, GelMA-COOH, and GelMA-DOPA (Figure S1); release of AMP (Figure S2); antimicrobial activity characterization (Figure S3); in vitro cytotoxicity and cellular evaluation (Figure S4); and primer sequences for qPCR experiments (Table S1) (PDF)

■ AUTHOR INFORMATION

Corresponding Authors
*N.A. e-mail: n.annabi@neu.edu.
*A.K. e-mail: alik@bwh.harvard.edu

ORCID ⓘ
Yu Shrike Zhang: 0000-0001-8642-133X
Ali Khademhosseini: 0000-0002-2692-1524

Author Contributions
H.C., K.Y., and M.K.-N contributed equally to this work.

Notes
The authors declare no competing financial interest.

■ REFERENCES

(1) Castellani, C.; Lindtner, R. A.; Hausbrandt, P.; Tschegg, E.; Stanzl-Tschegg, S. E.; Zanoni, G.; Beck, S.; Weinberg, A.-M. Bone−implant interface strength and osseointegration: Biodegradable magnesium alloy versus standard titanium control. *Acta Biomater.* **2011**, *7*, 432−440.

(2) Cui, C.; Hu, B.; Zhao, L.; Liu, S. Titanium alloy production technology, market prospects and industry development. *Mater. Eng.* **2011**, *32*, 1684−1691.

(3) Veiga, C.; Davim, J.; Loureiro, A. Properties and applications of titanium alloys: a brief review. *Rev. Adv. Mater. Sci.* **2012**, *32*, 133−148.

(4) Arciola, C. R.; Campoccia, D.; Speziale, P.; Montanaro, L.; Costerton, J. W. Biofilm formation in Staphylococcus implant infections. A review of molecular mechanisms and implications for biofilm-resistant materials. *Biomaterials* **2012**, *33*, 5967−5982.

(5) Zaat, S.; Broekhuizen, C.; Riool, M. Host tissue as a niche for biomaterial-associated infection. *Future Microbiol.* **2010**, *5*, 1149−1151.

(6) Zhao, L.; Wang, H.; Huo, K.; Cui, L.; Zhang, W.; Ni, H.; Zhang, Y.; Wu, Z.; Chu, P. K. Antibacterial nano-structured titania coating incorporated with silver nanoparticles. *Biomaterials* **2011**, *32*, 5706−5716.

(7) Cheng, H.; Xiong, W.; Fang, Z.; Guan, H.; Wu, W.; Li, Y.; Zhang, Y.; Alvarez, M. M.; Gao, B.; Huo, K.; et al. Strontium (Sr) and silver (Ag) loaded nanotubular structures with combined osteoinductive and antimicrobial activities. *Acta Biomater.* **2016**, *31*, 388−400.

(8) Kazemzadeh-Narbat, M.; Kindrachuk, J.; Duan, K.; Jenssen, H.; Hancock, R. E.; Wang, R. Antimicrobial peptides on calcium phosphate-coated titanium for the prevention of implant-associated infections. *Biomaterials* **2010**, *31*, 9519−9526.

(9) Ma, M.; Kazemzadeh-Narbat, M.; Hui, Y.; Lu, S.; Ding, C.; Chen, D. D.; Hancock, R. E.; Wang, R. Local delivery of antimicrobial peptides using self-organized TiO2 nanotube arrays for peri-implant infections. *J. Biomed. Mater. Res., Part A* **2012**, *100A*, 278−285.

(10) Kazemzadeh-Narbat, M.; Lai, B. F.; Ding, C.; Kizhakkedathu, J. N.; Hancock, R. E.; Wang, R. Multilayered coating on titanium for controlled release of antimicrobial peptides for the prevention of implant-associated infections. *Biomaterials* **2013**, *34*, 5969−5977.

(11) Kazemzadeh-Narbat, M.; Wang, Q.; Hancock, R. E.; Wang, R. Antimicrobial peptide delivery from trabecular bone grafts. *J. Biomater. Tissue Eng.* **2014**, *4*, 967−972.

(12) Muszanska, A. K.; Busscher, H. J.; Herrmann, A.; van der Mei, H. C.; Norde, W. Pluronic−lysozyme conjugates as anti-adhesive and antibacterial bifunctional polymers for surface coating. *Biomaterials* **2011**, *32*, 6333−6341.

(13) Zahran, M.; Ahmed, H. B.; El-Rafie, M. Surface modification of cotton fabrics for antibacterial application by coating with AgNPs−alginate composite. *Carbohydr. Polym.* **2014**, *108*, 145−152.

(14) Shah, N. J.; Hyder, M. N.; Moskowitz, J. S.; Quadir, M. A.; Morton, S. W.; Seeherman, H. J.; Padera, R. F.; Spector, M.; Hammond, P. T. Surface-Mediated Bone Tissue Morphogenesis from Tunable Nanolayered Implant Coatings. *Sci. Transl. Med.* **2013**, *5*, 191ra83.

(15) Chien, C.-Y.; Tsai, W.-B. Poly(dopamine)-Assisted Immobilization of Arg-Gly-Asp Peptides, Hydroxyapatite, and Bone Morphogenic Protein-2 on Titanium to Improve the Osteogenesis of Bone Marrow Stem Cells. *ACS Appl. Mater. Interfaces* **2013**, *5*, 6975−6983.

(16) Nguyen, A. H.; McKinney, J.; Miller, T.; Bongiorno, T.; McDevitt, T. C. Gelatin methacrylate microspheres for controlled growth factor release. *Acta Biomater.* **2015**, *13*, 101−110.

(17) Tsai, W.-B.; Chen, R. P.-Y.; Wei, K.-L.; Tan, S.-F.; Lai, J.-Y. Modulation of RGD-Functionalized Polyelectrolyte Multilayer Membranes for Promoting Osteoblast Function. *J. Biomater. Sci., Polym. Ed.* **2010**, *21*, 377−394.

(18) Tang, W.; Policastro, G. M.; Hua, G.; Guo, K.; Zhou, J.; Wesdemiotis, C.; Doll, G. L.; Becker, M. L. Bioactive Surface Modification of Metal Oxides via Catechol-Bearing Modular Peptides: Multivalent-Binding, Surface Retention, and Peptide Bioactivity. *J. Am. Chem. Soc.* **2014**, *136*, 16357−16367.

(19) Meng, Y.; Li, X.; Li, Z.; Liu, C.; Zhao, J.; Wang, J.; Liu, Y.; Yuan, X.; Cui, Z.; Yang, X. Surface Functionalization of Titanium Alloy with miR-29b Nanocapsules To Enhance Bone Regeneration. *ACS Appl. Mater. Interfaces* **2016**, *8*, 5783−5793.

(20) Lai, J.-Y. Biocompatibility of chemically cross-linked gelatin hydrogels for ophthalmic use. *J. Mater. Sci.: Mater. Med.* **2010**, *21*, 1899−1911.

(21) Monteiro, I. P.; Shukla, A.; Marques, A. P.; Reis, R. L.; Hammond, P. T. Spray-assisted layer-by-layer assembly on hyaluronic acid scaffolds for skin tissue engineering. *J. Biomed. Mater. Res., Part A* **2015**, *103*, 330−340.

(22) Lee, B. P.; Messersmith, P. B.; Israelachvili, J. N.; Waite, J. H. Mussel-inspired adhesives and coatings. *Annu. Rev. Mater. Res.* **2011**, *41*, 99.

(23) Lee, H.; Scherer, N. F.; Messersmith, P. B. Single-molecule mechanics of mussel adhesion. *Proc. Natl. Acad. Sci. U. S. A.* **2006**, *103*, 12999−13003.

(24) Lee, H.; Dellatore, S. M.; Miller, W. M.; Messersmith, P. B. Mussel-inspired surface chemistry for multifunctional coatings. *Science* **2007**, *318*, 426−430.

(25) Lee, H.; Lee, B. P.; Messersmith, P. B. A reversible wet/dry adhesive inspired by mussels and geckos. *Nature* **2007**, *448*, 338−341.

(26) Hong, S.; Pirovich, D.; Kilcoyne, A.; Huang, C.-H.; Lee, H.; Weissleder, R. Supramolecular Metallo-Bioadhesive for Minimally Invasive Use. *Adv. Mater.* **2016**, *28*, 8675−8680.

(27) Cong, Y.; Xia, T.; Zou, M.; Li, Z.; Peng, B.; Guo, D.; Deng, Z. Mussel-inspired polydopamine coating as a versatile platform for synthesizing polystyrene/Ag nanocomposite particles with enhanced antibacterial activities. *J. Mater. Chem. B* **2014**, *2*, 3450−3461.

(28) Sedó, J.; Saiz-Poseu, J.; Busqué, F.; Ruiz-Molina, D. Catechol-Based Biomimetic Functional Materials. *Adv. Mater.* **2013**, *25*, 653−701.

(29) Liu, Y.; Ai, K.; Lu, L. Polydopamine and Its Derivative Materials: Synthesis and Promising Applications in Energy, Environmental, and Biomedical Fields. *Chem. Rev.* **2014**, *114*, 5057−5115.

(30) Li, L.; Smitthipong, W.; Zeng, H. Mussel-inspired hydrogels for biomedical and environmental applications. *Polym. Chem.* **2015**, *6*, 353−358.

(31) Stepuk, A.; Halter, J. G.; Schaetz, A.; Grass, R. N.; Stark, W. J. Mussel-inspired load bearing metal-polymer glues. *Chem. Commun.* **2012**, *48*, 6238−6240.

(32) Bajaj, P.; Schweller, R. M.; Khademhosseini, A.; West, J. L.; Bashir, R. 3D biofabrication strategies for tissue engineering and regenerative medicine. *Annu. Rev. Biomed. Eng.* **2014**, *16*, 247.

(33) Chen, Y. C.; Lin, R. Z.; Qi, H.; Yang, Y.; Bae, H.; Melero-Martin, J. M.; Khademhosseini, A. Functional human vascular network generated in photocrosslinkable gelatin methacrylate hydrogels. *Adv. Funct. Mater.* **2012**, *22*, 2027−2039.

(34) Nichol, J. W.; Koshy, S. T.; Bae, H.; Hwang, C. M.; Yamanlar, S.; Khademhosseini, A. Cell-laden microengineered gelatin meth-acrylate hydrogels. *Biomaterials* **2010**, *31*, 5536−5544.

(35) Ganesh, N.; Jayakumar, R.; Koyakutty, M.; Mony, U.; Nair, S. V. Embedded silica nanoparticles in poly (caprolactone) nanofibrous scaffolds enhanced osteogenic potential for bone tissue engineering. *Tissue Eng., Part A* **2012**, *18*, 1867−1881.

(36) Gaharwar, A. K.; Kishore, V.; Rivera, C.; Bullock, W.; Wu, C. J.; Akkus, O.; Schmidt, G. Physically Crosslinked Nanocomposites from Silicate-Crosslinked PEO: Mechanical Properties and Osteogenic Differentiation of Human Mesenchymal Stem Cells. *Macromol. Biosci.* **2012**, *12*, 779−793.

(37) Gaharwar, A. K.; Mihaila, S. M.; Swami, A.; Patel, A.; Sant, S.; Reis, R. L.; Marques, A. P.; Gomes, M. E.; Khademhosseini, A. Bioactive silicate nanoplatelets for osteogenic differentiation of human mesenchymal stem cells. *Adv. Mater.* **2013**, *25*, 3329−3336.

(38) Loessner, D.; Meinert, C.; Kaemmerer, E.; Martine, L. C.; Yue, K.; Levett, P. A.; Klein, T. J.; Melchels, F. P.; Khademhosseini, A.; Hutmacher, D. W. Functionalization, preparation and use of cell-laden gelatin methacryloyl-based hydrogels as modular tissue culture platforms. *Nat. Protoc.* **2016**, *11*, 727−746.

(39) Zhang, Y.-N.; Avery, R. K.; Vallmajo-Martin, Q.; Assmann, A.; Vegh, A.; Memic, A.; Olsen, B. D.; Annabi, N.; Khademhosseini, A. A Highly Elastic and Rapidly Crosslinkable Elastin-Like Polypeptide-Based Hydrogel for Biomedical Applications. *Adv. Funct. Mater.* **2015**, *25*, 4814−4826.

(40) Shin, S. R.; Aghaei-Ghareh-Bolagh, B.; Dang, T. T.; Topkaya, S. N.; Gao, X.; Yang, S. Y.; Jung, S. M.; Oh, J. H.; Dokmeci, M. R.; Tang, X. S.; Khademhosseini, A. Cell-laden Microengineered and Mechanically Tunable Hybrid Hydrogels of Gelatin and Graphene Oxide. *Adv. Mater.* **2013**, *25*, 6385−6391.

(41) Shin, H.; Olsen, B. D.; Khademhosseini, A. The mechanical properties and cytotoxicity of cell-laden double-network hydrogels based on photocrosslinkable gelatin and gellan gum biomacromolecules. *Biomaterials* **2012**, *33*, 3143−3152.

(42) Panzavolta, S.; Gioffrè, M.; Focarete, M. L.; Gualandi, C.; Foroni, L.; Bigi, A. Electrospun gelatin nanofibers: optimization of genipin cross-linking to preserve fiber morphology after exposure to water. *Acta Biomater.* **2011**, *7*, 1702−1709.

(43) Jaiswal, A.; Chhabra, H.; Soni, V.; Bellare, J. Enhanced mechanical strength and biocompatibility of electrospun polycaprolactone-gelatin scaffold with surface deposited nano-hydroxyapatite. *Mater. Sci. Eng., C* **2013**, *33*, 2376−2385.

(44) Liao, H.; Walboomers, X. F.; Habraken, W. J.; Zhang, Z.; Li, Y.; Grijpma, D. W.; Mikos, A. G.; Wolke, J. G.; Jansen, J. A. Injectable calcium phosphate cement with PLGA, gelatin and PTMC microspheres in a rabbit femoral defect. *Acta Biomater.* **2011**, *7*, 1752−1759.

(45) Yue, K.; Trujillo-de Santiago, G.; Alvarez, M. M.; Tamayol, A.; Annabi, N.; Khademhosseini, A. Synthesis, properties, and biomedical applications of gelatin methacryloyl (GelMA) hydrogels. *Biomaterials* **2015**, *73*, 254−271.

(46) Nikkhah, M.; Eshak, N.; Zorlutuna, P.; Annabi, N.; Castello, M.; Kim, K.; Dolatshahi-Pirouz, A.; Edalat, F.; Bae, H.; Yang, Y.; Khademhosseini, A. Directed endothelial cell morphogenesis in micropatterned gelatin methacrylate hydrogels. *Biomaterials* **2012**, *33*, 9009−9018.

(47) Jia, W.; Gungor-Ozkerim, P. S.; Zhang, Y. S.; Yue, K.; Zhu, K.; Liu, W.; Pi, Q.; Byambaa, B.; Dokmeci, M. R.; Shin, S. R.; Khademhosseini, A. Direct 3D Bioprinting of Perfusable Vascular Constructs Using a Blend Bioink. *Biomaterials* **2016**, *106*, 58−68.

(48) Saxer, S.; Portmann, C.; Tosatti, S.; Gademann, K.; Zurcher, S.; Textor, M. Surface assembly of catechol-functionalized poly (l-lysine)-graft-poly (ethylene glycol) copolymer on titanium exploiting combined electrostatically driven self-organization and biomimetic strong adhesion. *Macromolecules* **2010**, *43*, 1050−1060.

(49) You, I.; Kang, S. M.; Byun, Y.; Lee, H. Enhancement of blood compatibility of poly (urethane) substrates by mussel-inspired adhesive heparin coating. *Bioconjugate Chem.* **2011**, *22*, 1264−1269.

(50) Zvarec, O.; Purushotham, S.; Masic, A.; Ramanujan, R. V.; Miserez, A. Catechol-functionalized chitosan/iron oxide nanoparticle composite inspired by mussel thread coating and squid beak interfacial chemistry. *Langmuir* **2013**, *29*, 10899−10906.

(51) Lee, H. J.; Koo, A. N.; Lee, S. W.; Lee, M. H.; Lee, S. C. Catechol-functionalized adhesive polymer nanoparticles for controlled local release of bone morphogenetic protein-2 from titanium surface. *J. Controlled Release* **2013**, *170*, 198−208.

(52) Kang, S. M.; Park, S.; Kim, D.; Park, S. Y.; Ruoff, R. S.; Lee, H. Simultaneous Reduction and Surface Functionalization of Graphene Oxide by Mussel-Inspired Chemistry. *Adv. Funct. Mater.* **2011**, *21*, 108−112.

(53) Salwiczek, M.; Qu, Y.; Gardiner, J.; Strugnell, R. A.; Lithgow, T.; McLean, K. M.; Thissen, H. Emerging rules for effective antimicrobial coatings. *Trends Biotechnol.* **2014**, *32*, 82−90.

(54) Cloutier, M.; Mantovani, D.; Rosei, F. Antibacterial Coatings: Challenges, Perspectives, and Opportunities. *Trends Biotechnol.* **2015**, *33*, 637−652.

(55) Mihaila, S. M.; Gaharwar, A. K.; Reis, R. L.; Khademhosseini, A.; Marques, A. P.; Gomes, M. E. The osteogenic differentiation of SSEA-4 sub-population of human adipose derived stem cells using silicate nanoplatelets. *Biomaterials* **2014**, *35*, 9087−9099.

(56) Xavier, J. R.; Thakur, T.; Desai, P.; Jaiswal, M. K.; Sears, N.; Cosgriff-Hernandez, E.; Kaunas, R.; Gaharwar, A. K. Bioactive nanoengineered hydrogels for bone tissue engineering: a growth-factor-free approach. *ACS Nano* **2015**, *9*, 3109−3118.

(57) Trappmann, B.; Gautrot, J. E.; Connelly, J. T.; Strange, D. G.; Li, Y.; Oyen, M. L.; Cohen Stuart, M. A.; Boehm, H.; Li, B.; Vogel, V.; et al. Extracellular-matrix tethering regulates stem-cell fate. *Nat. Mater.* **2012**, *11*, 642−649.

(58) Engler, A. J.; Griffin, M. A.; Sen, S.; Bönnemann, C. G.; Sweeney, H. L.; Discher, D. E. Myotubes differentiate optimally on substrates with tissue-like stiffness: pathological implications for soft or stiff microenvironments. *J. Cell Biol.* **2004**, *166*, 877−887.

(59) Rupp, F.; Scheideler, L.; Olshanska, N.; de Wild, M.; Wieland, M.; Geis-Gerstorfer, J. Enhancing surface free energy and hydrophilicity through chemical modification of microstructured titanium implant surfaces. *J. Biomed. Mater. Res., Part A* **2006**, *76A*, 323−334.

(60) Annabi, N.; Shin, S. R.; Tamayol, A.; Miscuglio, M.; Bakooshli, M. A.; Assmann, A.; Mostafalu, P.; Sun, J.-Y.; Mithieux, S.; Cheung, L.; Tang, X.; Weiss, A. S.; Khademhosseini, A. Highly Elastic and Conductive Human-Based Protein Hybrid Hydrogels. *Adv. Mater.* **2016**, *28*, 40−49.

(61) Gong, J. P. Why are double network hydrogels so tough? *Soft Matter* **2010**, *6*, 2583−2590.

(62) Hilpert, K.; Elliott, M.; Jenssen, H.; Kindrachuk, J.; Fjell, C. D.; Körner, J.; Winkler, D. F. H.; Weaver, L. L.; Henklein, P.; Ulrich, A. S.; Chiang, S. H. Y.; Farmer, S. W.; Pante, N.; Volkmer, R.; Hancock, R. E. W. Screening and Characterization of Surface-Tethered Cationic Peptides for Antimicrobial Activity. *Chem. Biol.* **2009**, *16*, 58−69.

(63) Boulos, L.; Prévost, M.; Barbeau, B.; Coallier, J.; Desjardins, R. LIVE/DEAD® BacLight: application of a new rapid staining method for direct enumeration of viable and total bacteria in drinking water. *J. Microbiol. Methods* **1999**, *37*, 77−86.

(64) Zhao, L.; Chu, P. K.; Zhang, Y.; Wu, Z. Antibacterial coatings on titanium implants. *J. Biomed. Mater. Res., Part B* **2009**, *91B*, 470−480.

(65) Pagel, M.; Hassert, R.; John, T.; Braun, K.; Wießler, M.; Abel, B.; Beck-Sickinger, A. G. Multifunctional Coating Improves Cell Adhesion on Titanium by using Cooperatively Acting Peptides. *Angew. Chem., Int. Ed.* **2016**, *55*, 4826−4830.

(66) Goodman, S. B.; Yao, Z.; Keeney, M.; Yang, F. The future of biologic coatings for orthopaedic implants. *Biomaterials* **2013**, *34*, 3174−3183.

(67) Bose, S.; Fielding, G.; Tarafder, S.; Bandyopadhyay, A. Understanding of dopant-induced osteogenesis and angiogenesis in calcium phosphate ceramics. *Trends Biotechnol.* **2013**, *31*, 594−605.

(68) Qin, X.; Jiang, Q.; Matsuo, Y.; Kawane, T.; Komori, H.; Moriishi, T.; Taniuchi, I.; Ito, K.; Kawai, Y.; Rokutanda, S.; et al. Cbfb regulates bone development by stabilizing Runx family proteins. *J. Bone Miner. Res.* **2015**, *30*, 706−714.

(69) Ricarte, F.; Nakatani, T.; Partridge, N. PTH Signaling and Epigenetic Control of Bone Remodeling. *Curr. Mol. Biol. Rep.* **2016**, *2*, 56−61.

(70) Raphel, J.; Holodniy, M.; Goodman, S. B.; Heilshorn, S. C. Multifunctional coatings to simultaneously promote osseointegration and prevent infection of orthopaedic implants. *Biomaterials* **2016**, *84*, 301−314.